Supporting Information

Rational Interface-Enriched Defects Induce Excellent Thermoelectric Performance of Sandwich-Type $Ca_3Co_4O_9$ Textured Composites

Zongmo Shi[1, 4], Zhen Han[1], Wei Huang[2*], Jie Xu[3], Yuan Liu[1], Ying Zhang[1], Chanli Chen[1], Jian Wei[1, 4*], Geping He[1], Junzhan Zhang[1]

1 College of Materials Science and Engineering, Xi'an University of Architecture and Technology, Xi'an, 710055, P. R. China

2 College of Civil Engineering, Xi'an University of Architecture & Technology, Xi'an 710055, P. R.China

3 State Key Laboratory of Solidification Processing, MIIT Key laboratory of Radiation Detection Materials and Devices, USI Institute of Intelligence Materials and Structure, NPU-QMUL Joint Research Institute of Advanced Materials and Structure, School of Material Science and Engineering, Northwestern Polytechnical University, Xi'an, 710072, P. R. China

4 Shaanxi Key Laboratory of Nano Materials and Technology, Xi'an, 710055, P. R. China

[*] Corresponding author
E-mail: qqhuangwei2005@126.com, Tel: +86-29-82205328
[*] Corresponding author
E-mail: weijian@xauat.edu.cn Tel: +86-29-82205395

Figure S1 shows the SEM image and corresponding EDS elemental mappings of textured composites. It is found that the recrystallization process of template seeds additives induced the directional alignment of the matrix grains along the (00*l*) atomic plane. The compact grain boundary hindered defect diffusion and led to the low resistance of grain boundaries for textured composites. An obvious Ag phase segregation was observed and the $Ca_{2.87}Ag_{0.1}La_{0.03}Co_4O_9$ grains arranged tightly in the both sides of the Ag layer, which were presented in Figure S1 (f) - (m).

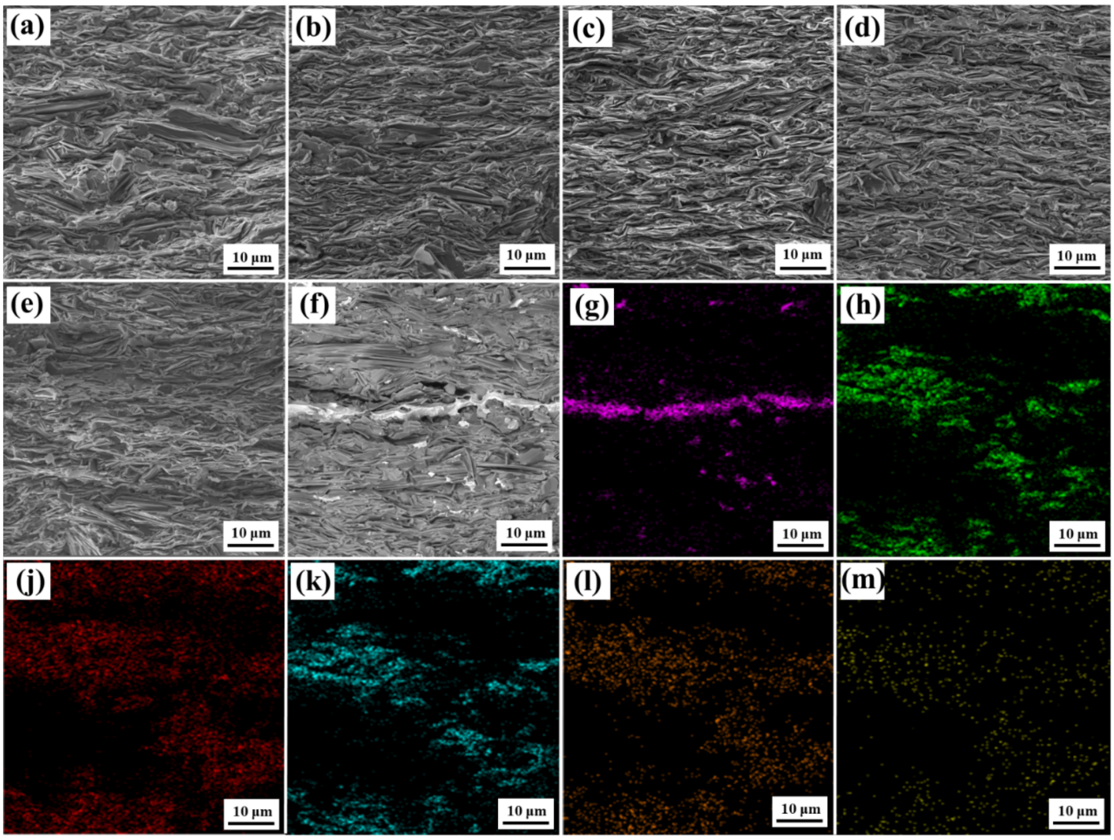

Figure S1 SEM images of the textured ceramics with different silver layers. (a) n=0, (b) n=1, (c) n=2, (d) n=3, (e) n=5, (f) silver layer, (g) EDX mapping for Ag element, (h) EDX mapping for Ca element, (j) EDX mapping for O element, (k) EDX mapping for Co element, (l) EDX mapping for Bi element, (m) EDX mapping for La element

As shown the EBSD results of Figure S2 (a), the numerous fine grains were formed, which could be mainly ascribed to preferential occurrence of grain growth along the (00*l*) plane during the texture evolution process. The grain sizes presented the homogenized distribution. Besides, the fine grains were believed to be the recrystallized ones according to geometrically necessary dislocations (refer to Figure S2 (c)). The results of pole figures showed a higher concentrated distribution along the (00*l*) direction, which were corresponded to the high (00*l*) peaks intensity of XRD results.

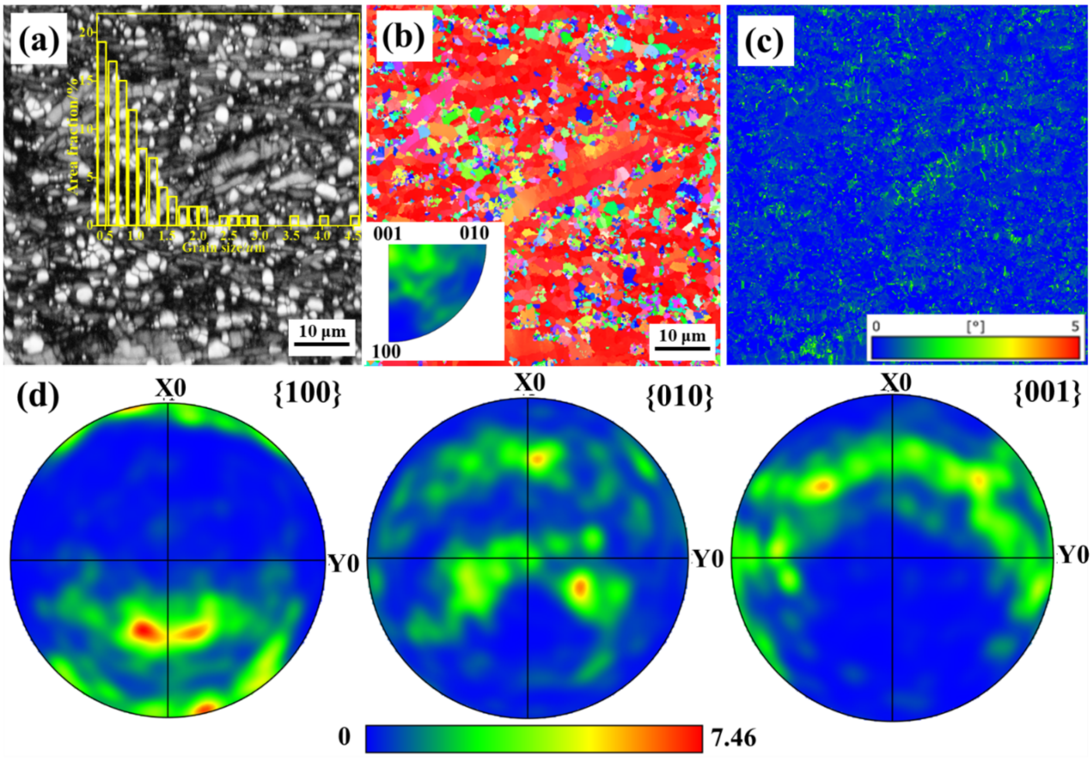

Figure S2 EBSD results of textured composites with double-layered sliver additives. (a) Diffraction band contrast image and grain size distribution, (b) Z-Euler image, inverse pole figures (IPF) is inset, (c) Geometrically necessary dislocations (GND), (d) pole figures along (100), (010), and (001) direction

Figure S3 presented the interface between textured grains and sliver layer in the textured composites, which was fabricated by FIB technology. It could be used for the atomic-scale structural defects analysis of the composite sample.

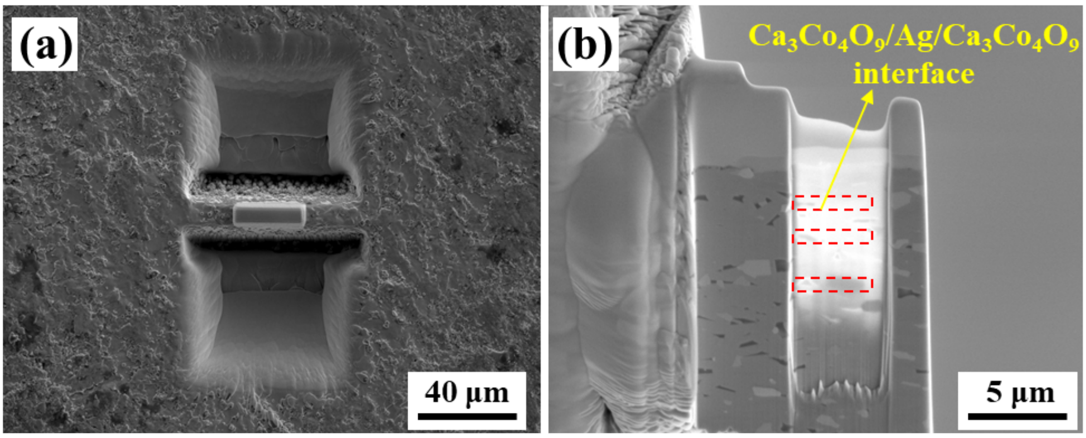

Figure S3 Interface between textured grains and sliver layer in the textured composites fabricated by FIB technology.

Figure S4 shows HAADF STEM image of the n=2 sample. The additional [Ca_2CoO_3] layer and [CoO_2] layer were semi-coherently intercalated in $Ca_3Co_4O_9$ lattice and the SAED pattern along $[100]_c$, revealing the stacking order along the crystallographic c-axis. Interestingly, the enlarged images in Figure S4 (b) and (c) from the different region clearly resolved the atom columns locating at the center of the matrix cells. The high density dislocations were found in the sample, which could be verified by Figure S4 (d), as showing the HAADF STEM image and SAED pattern along $[111]_c$.

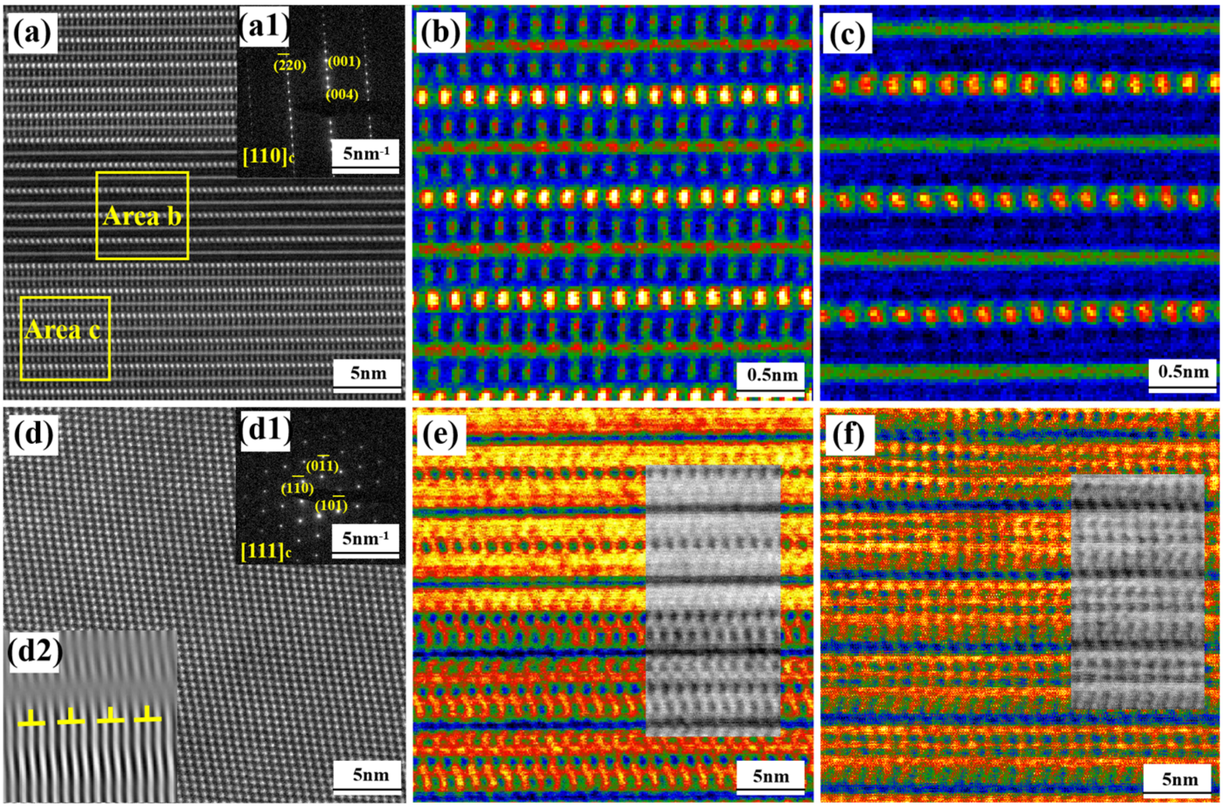

Figure S4 Atomically resolved interfacial structure of the composites with double-layered sliver additives. (a) Atomically resolved STEM HAADF image along [110] zone axis with its electron diffraction pattern (inset (a1)), (b) Atomically resolved STEM HAADF images for Area b, of the interface between lamellae-shape sliver precipitates and the matrix. (c) Atomically-resolved STEM HAADF images of the $Ca_{2.87}Ag_{0.1}La_{0.03}Co_4O_9$ matrix, showing ordered element doping, (d) Atomically resolved STEM HAADF image of the 2SL sample along [111] zone axis with its electron diffraction pattern (inset (d1)), the inset (d2) shows the its the fast Inverse Fourier transform (IFFT) image, (e) Atomically-resolved STEM ABF image along [110] zone axis from the interface, (f) Atomically-resolved STEM ABF image along [110] zone axis from the $Ca_{2.87}Ag_{0.1}La_{0.03}Co_4O_9$ matrix

XPS spectra were used to verify the surface chemistry of the composites. Figure S5 (a) shows the full spectra of the samples, which presented the Ag 3*d*, Co 2*p*, Ca 2*s*, Ca 3*s*, Ca 2*p*, O 1*s*, O KLL binding energy peaks. In Figure S5 (b), the Co^{3+} and Co^{4+} ions were coexisted in the samples. In addition, the binding energies the O 1*s* peaks shifted to lower due to the additive of sliver layers in the $Ca_{2.87}Ag_{0.1}La_{0.03}Co_4O_9$/Ag/$Ca_{2.87}Ag_{0.1}La_{0.03}Co_4O_9$ composites.

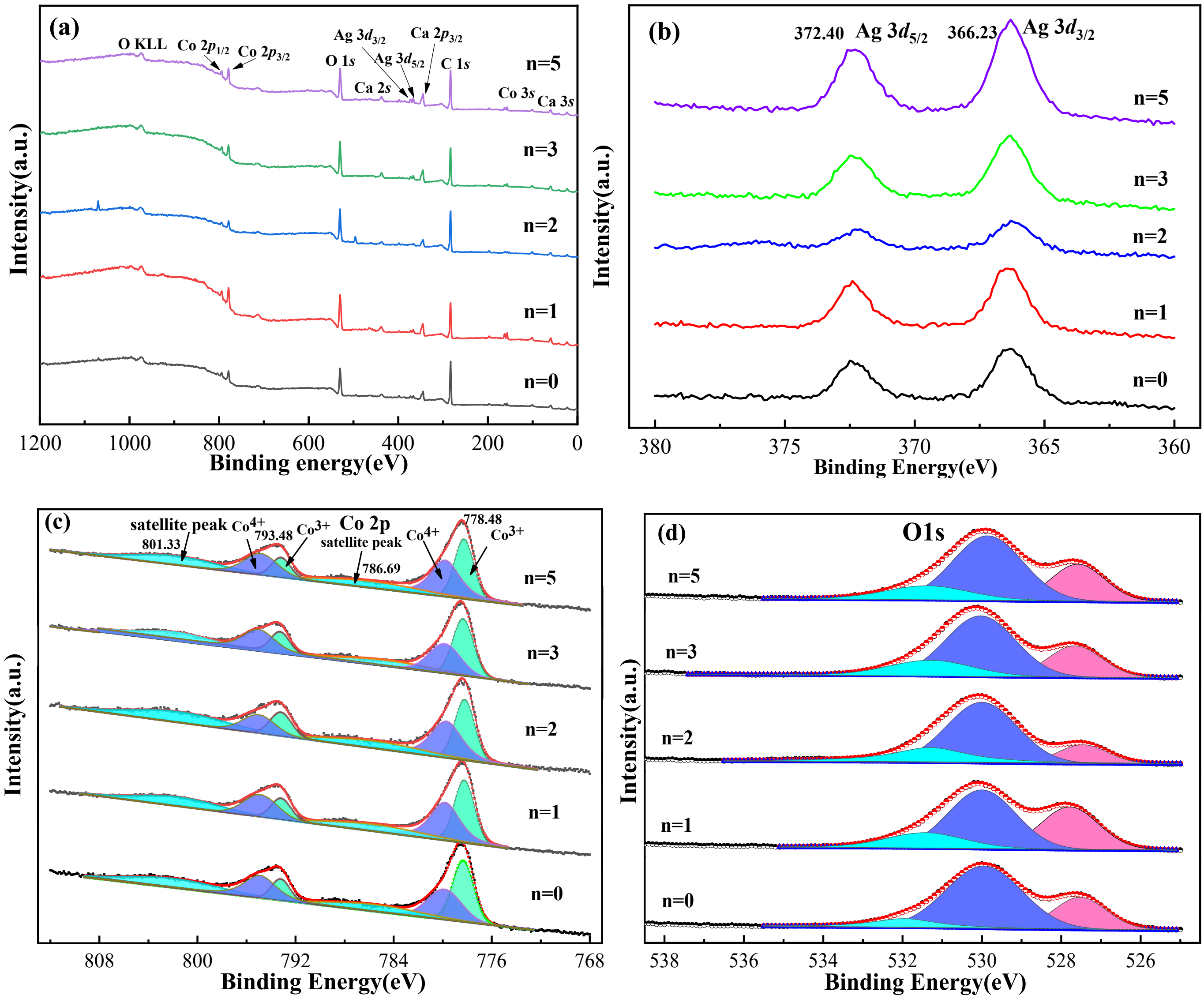

Figure S5 XPS spectra of the textured composites with different sliver layers. (a) full spectra, (b) Ag 3*d* peak, (c) Co 2*p* peak, (d) O 1*s* peak